Bachelor Thesis

Stockholm University

Degree Project in
Geology 15 hp

Crystal Size Distribution and Geochemical Analysis: Plagioclase Populations in volcanic rocks from Givshad (Iran)

Tasmia Shafiq Naushad

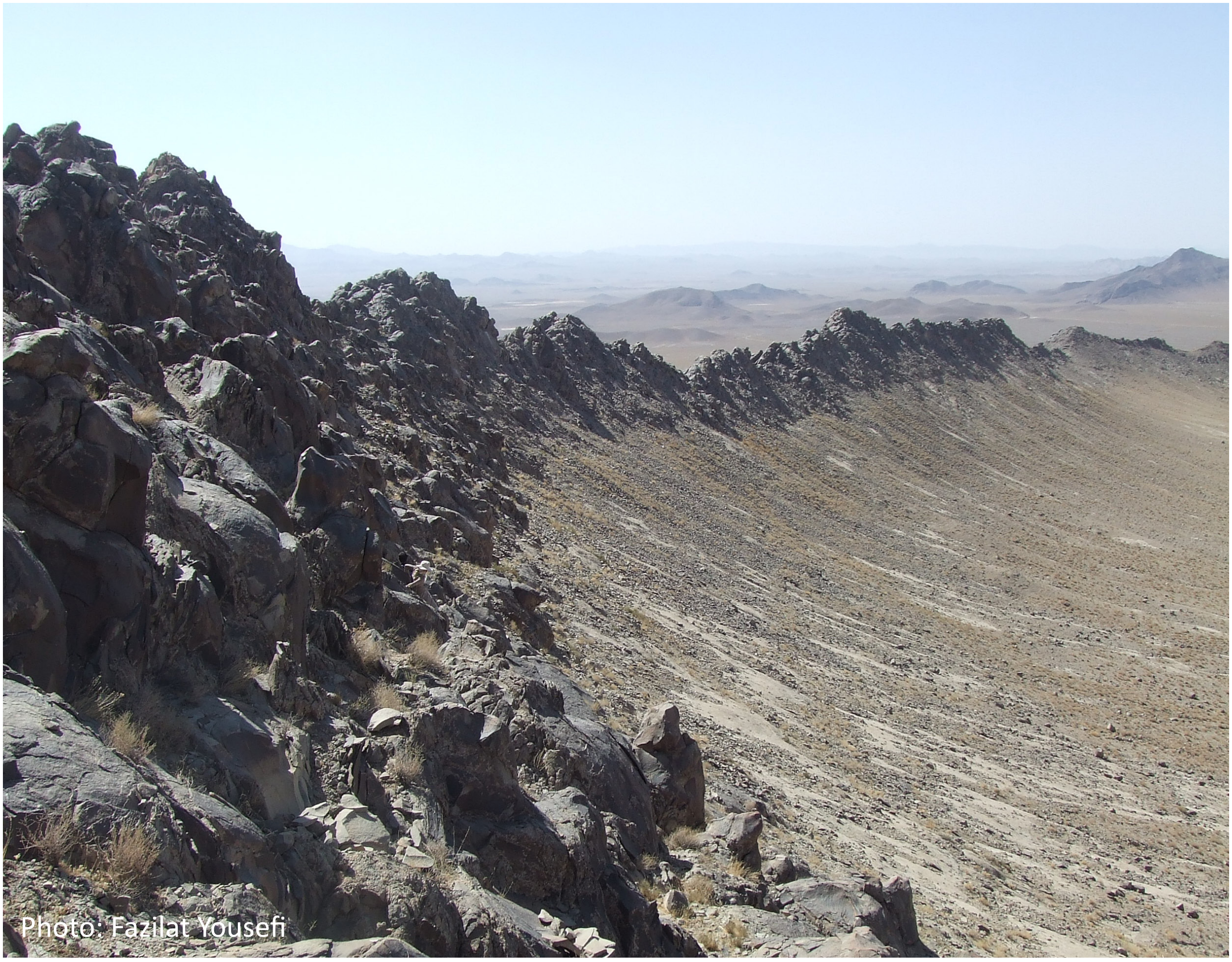

Stockholm 2023

Department of Geological Sciences
Stockholm University
SE-106 91 Stockholm

Abstract

This study presents petrographic, geochemical, and crystal size distribution analyses of plagioclase populations in four samples collected from the volcanic structure (Aghol Kuh) near Givshad, Eastern-Iran. The aim was to investigate the magmatic processes and potential eruption triggers associated with this structure. The results reveal the presence of two distinct plagioclase populations, suggesting the phenomena of magma mixing prior to the eruption event. This finding proposes that a mixing event could have acted as a trigger to the final eruption. To further support this conclusion, additional quantitative geochemical investigations incorporating isotopic and trace elemental analysis are recommended. These additional studies would provide valuable insights into the specific processes and mechanisms involved in magma mixing. The comprehensive understanding of these processes is essential for assessing volcanic hazards and developing effective mitigation measures.

Keywords: Crystal size distribution (CSD); Energy dispersive x-ray spectroscopy (EDS); Plagioclase; Disequilibrium-textures; Magma-mixing

Independent Project in Geological Science, GG6113, 15 credits, 2023
Supervisor: Victoria Pease
Department of Geological Sciences, Stockholm University, Svante Arrhenius väg 8, SE-114 18 Stockholm (www.su.se/department-of-geological-sciences)

Contents

1 Introduction **1**
1.1 Crystal size distribution . . . 1
1.2 Igneous microtextures . . . 2
1.2.1 Porphyritic rocks . . . 2
1.2.2 Zoning and disequilibrium textures . . . 4

2 Geological Background **6**
2.1 Sistan suture zone . . . 6
2.2 Petrography . . . 6

3 Methods **9**
3.1 Crystal Size Distribution . . . 9
3.2 Geochemical Analysis . . . 10

4 Results **11**
4.1 CSD Analysis . . . 11
4.2 SEM-EDS Analysis . . . 11

5 Discussion **16**
5.1 Integration of CSD and EDS . . . 16
5.2 Magmatism of the Givshad structure . . . 17
5.3 Future work . . . 17
5.4 Conclusions . . . 18

Acknowledgements **19**

References **20**

Appendix **22**

Introduction

Quantitative textural analysis is applied to study magma chamber processes such as nucleation, growth rates, resident times, magma mixing and textural coarsening. Investigating these processes reveal information that can assist developing effective mitigation measures against volcanic hazards by, e.g. identifying eruptive triggers. Of particular interest are the processes associated with the refilling of a cooler felsic magma chamber by a hotter, more mafic magma, as it has been attributed to the most violent and catastrophic volcanic eruptions (Morgavi et al., 2017).

In this thesis, plagioclase crystals in volcanic rocks from near Givshad (Eastern-Iran) are investigated using quantitative textural statistical analysis and semi quantitative compositional mapping integrated with qualitative petrological observations of microtextures. The aim is to define if plagioclase crystals represent one or several crystal-size populations and use this information to gain potential insight about the magmatism related to the Givshad volcanic structure (locally called Aghol Kuh). The results of this work document at least two crystal size populations that, when combined with crystal compositional mapping, indicate mafic magma recharge as a possible eruptive mechanism.

1.1 Crystal size distribution

In igneous petrology, crystal size distribution (CSD) developed when Marsh and Cashman applied the CSD method to basaltic rocks (Cashman & Marsh, 1988; Marsh, 1988). It represents the number of crystals per unit volume within defined size intervals, which can be refined for a smoother representation with increased measurements (Higgins, 2006b). Marsh's model showed that the CSD for continuous crystallization in an open steady state system defines a straight line when plotting population density, ln (n) against crystal size (L) given by:

$$ln(n) = ln(n^0) - L/G\tau$$

where nucleation density (n^0) is the intercept given at L=0, and the slope of the line is defined by the reciprocal product of growth rate (G) and residence time (τ) i.e. $1/G\tau$.

It was also shown that in closed system crystallization, in response to linearly increasing undercooling, linear CSDs were generated. However, they can follow any function, and studies describing these models have generated idealized CSD plots (Figure 1). The shapes of CSD plots can be related to crystallization processes because, in both steady state and time dependent systems, the slope of the CSD trend is determined by the nucleation density (intercept = $ln(n^0)$) and the crystal growth rate ($1/G\tau$). For instance, if liquid is removed from the system, the nucleation rate is reduced which is accompanied by a depletion in smaller crystal sizes (Boorman et al., 2004). These techniques can be used to determine magma processes such as batch crystallization, magma-mixing, and provide information on crystal growth rates and residence times (Marsh, 1988, 1998).

There are several challenges related to CSD analysis. For instance, crystal size needs to be determined and uncertainties can occur when measuring several populations of heterogeneous crystal shapes. To ensure accuracy, stereology corrections are recommended to best fit the crystals in question (Cashman, 2020), otherwise, interpretations of the analysis should be reviewed with caution. Technically, crystal size is an intensive property described in three dimensions (Higgins, 2006a), and so a stereological correction is needed to convert 2D-measurements from thin-sections into 3D; The classic area-to-volume correction was first used by Wager (1961):

$$n_V(L_{XY}) = n_A(l_{XY})^{1.5}$$

where $n_V(L_{XY})$ is the number of crystals per unit volume in the length interval L_X to L_Y, and $n_A(l_{XY})$ is the number of intersections per unit area in the intersection length interval l_X to l_Y. Higgins (2000) advised against this method and incorporated a new method into CSDCorrections, a software package for CSD analysis. Today's standard incorporates w/l distribution models in the CSDCorrections program, however, estimates of crystal shape and fabric are still needed for accurate CSD calculations. Previous studies commonly use CSDSlice (Morgan & Jerram, 2006) to determine ratios for crystal habit. Jaret et al. (2008) compared 2D-3D conversion methodologies involving the classic area-to-volume correction, CSDCorrections only, and the third using both CSDCorrection and CSDSlice. They concluded that the last method was the most accurate in producing high quality results. However, CSDSlice does not include the same crystal shape library as CSDCorrections. Therefore, ShapeCalc was introduced by Mangler et al. (2022). For consistent results, the authors suggested using the newly developed program for 3D shape estimates, relative to CSDSlice since it uses the same w/l distribution models as CSDCorrections.

Moreover, since CSD plots are given by size intervals represented by points, non-unique line-fits allow numerous interpretations of the same data. Another difficulty mentioned by Cashman (2020) is to which extent natural volcanic systems differ from steady state industrial crystallization, which ultimately the modeling is based on. This could cause misconceptions, and therefore it is advised to integrate CSD-analysis with other geological observations or methods to assure an accurate assessment.

1.2 Igneous microtextures

1.2.1 Porphyritic rocks

Volcanic rocks often consists of relatively large crystals (phenocrysts) in a finer-grained groundmass (Vernon, 2004). The absolute grain size is variable, however, porphyritic textures commonly occur in volcanic and shallow intrusive rocks, in contrast to deeper coarser-grained intrusive rocks. Generally, porphyritic textures are interpreted to represent slow crystallization at depth growing the phenocryst

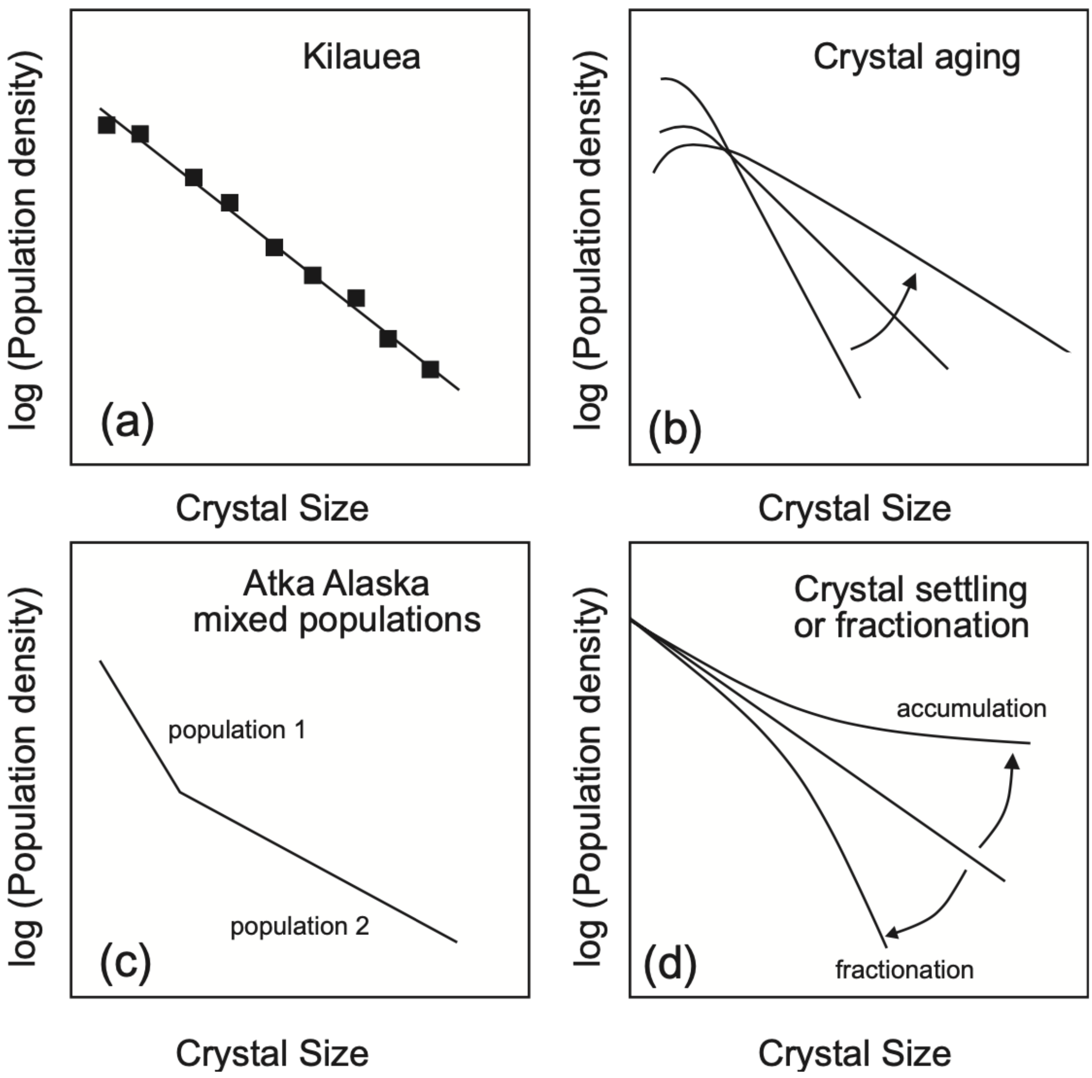

Figure 1: Idealized CSD plots illustrating the effect of different crystallization processes on CSD profiles by Boorman et al. (2004). (a) Straight linear trend commonly seen in quickly-cooled samples, example from the 1959 eruption of Kilauea (Cashman, 1990). (b) Counter-clockwise spin yielding decreasing fractions of small size intervals, expected from textural coarseing (Higgins, 1999). (c) Kinked trend expected from mixed populations from Atka, Alaska (Resmini, 1993). (d) Effect of crystal fractionation (loss of larger size intervals) and crystal accumulation (preferential settling of larger grains) comparative to an initially log-linear profile (Marsh, 1988)

.

phase(s) and later rapid cooling due to eruption or intrusion to colder rocks, producing the finer-grained groundmass. However, porphyritic rocks can also be formed in a single event confirmed by experiments conducted by Lofgren (1980) and Swanson (1977). This process can be observed in basalts when the first precipitating mineral, e.g. pyroxene, crystallizes alone for some time, making the adjacent melt supersaturated with the other ions causing another mineral, e.g. plagioclase, to form. When the late mineral finally crystallizes, it precipitates as abundant small crystals enclosing the earlier pyroxene phenocrysts.

1.2.2 Zoning and disequilibrium textures

Compositional zoning in igneous minerals is common in those that belong to a solid-solution series (Vernon, 2004). These minerals are continuously in exchange with the melt surrounding them. Complete equilibrium between the melt and a growing crystal should produce a compositionally uniform crystal. However, both diffusion and ion exchange are significantly slow, and temperature is not necessarily constant, which constrains crystal composition during growth under varying conditions. The rim is the only part of a crystal that equilibrates with the melt, resulting in compositional zoning during the cooling history of the crystal. Plagioclase often demonstrates this compositional variation, which depends on the substitution of Ca+Al and Na+Si. In contrast, reverse zoning exhibits the opposite compositional trend, with crystals becoming more enriched in calcium from core to rim. This microtexture is often related to magma recharge which refers to injection of mafic hotter magma into cooler felsic magma (Vernon, 2004).

Oscillatory zoning is common in plagioclase crystals, and is generally considered to be an equilibrium texture (Vernon, 2004). It involves small compositional changes during the growth of the crystals due to diffusion in the melt rather than temperature fluctuations, which produces a distinct pattern of alternating calcium composition. However, complex oscillatory zoning could occur due to repeating resorption and growth processes indicating disequilibrium conditions during magma mixing (Perugini & Poli, 2012).

Other disequilibrium textures are skeletal habits, sieve/spongy textures, and patchy zoning (Hibbard, 1981; Nelson & Montana, 1992; Vance, 1965). All have been associated with magmatic processes including magma mixing. Plagioclase grains of calcic dendritic overgrowth on sodic corroded cores suggest rapid precipitation resulting from strong undercooling and compositional change of the melt due to mixing (Hibbard, 1981). Undercooling is often related to fast cooling seen in rapid eruption, fast quenching, or interaction with a cooler medium; yielding glassy textures, resorption features, or complex zoning patterns. These conditions could also yield sieve textures, which preserve interconnected melt inclusions within the crystal structure creating a porous or sieve-like appearance (Nelson & Montana, 1992). Comparatively, patchy zoning refers to the occurrence of irregularly shaped and discontinuous zones within plagioclase (Vance, 1965). They reveal different compositions or optical properties relative to the surrounding area. Disequilibrium textures are considered to indicate magma mixing, however other sources of evidence such as major and trace element data, or other geological observations should be implemented when evaluating magmatic processes (Perugini & Poli, 2012).

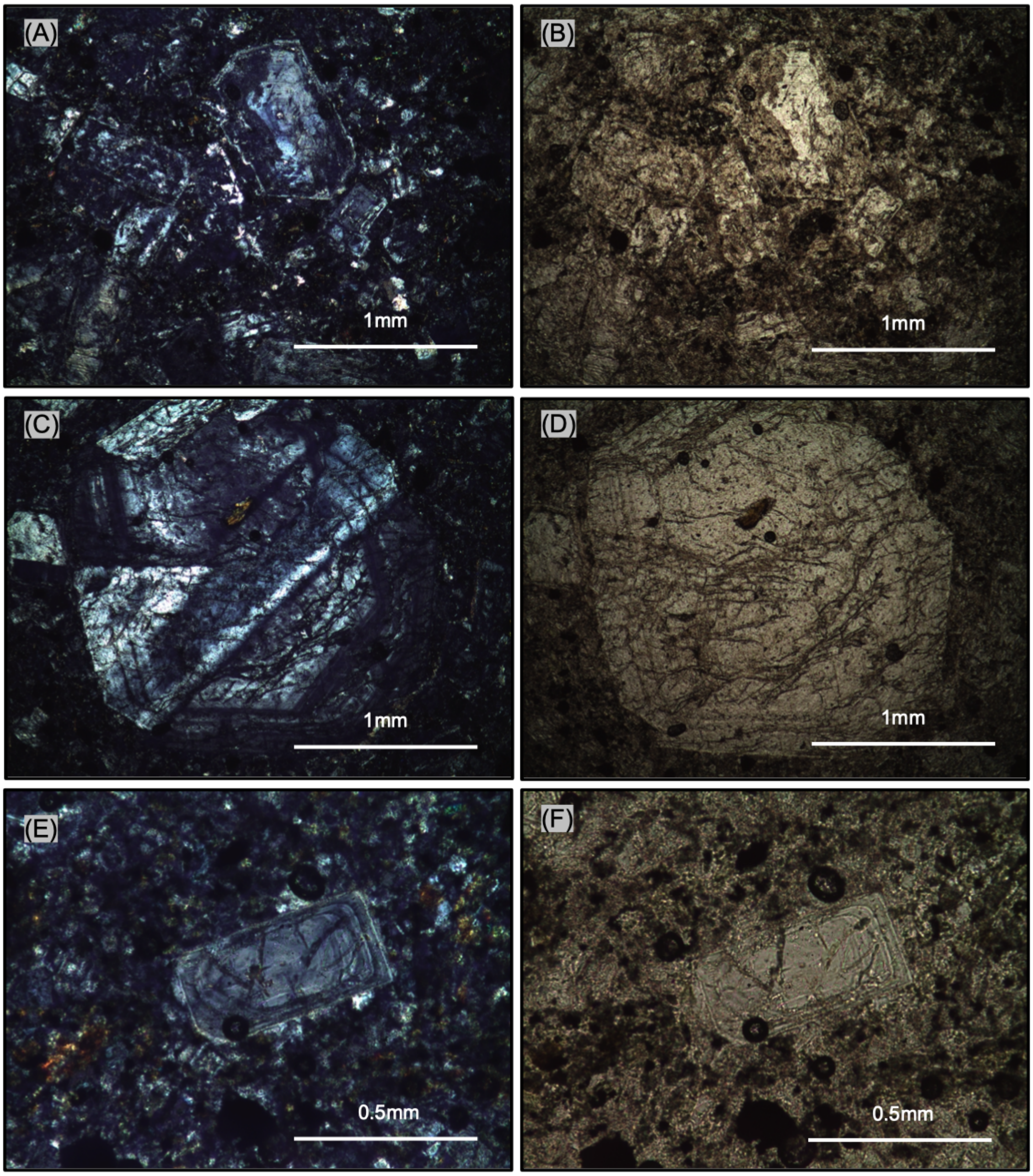

Figure 2: Microphotographs of plagioclase textures. Cross-polarized light (XPL) to the left, plane-polarized light (PPL) to the right. (A)-(B) Oscillatory zoned core with sieve textured layer and bright rim, sample G4. (C)-(D) Complex oscillatory zoning + resorption textures in large crystal, sample G2. (E)-(F) Oscillatory zoning in resorbed core, which evolves to an equant rim, sample G2.

Geological Background

2.1 Sistan suture zone

The study area is near the Sistan suture zone (31 to 35 °N and 57 to 61 °E) in Eastern Iran where a complex history of diverse geologic settings dating back to the closing of the Neotethyan ocean basin between the Central Iranian Lut block and the Afghan microcontinent are preserved (Bröcker et al., 2022). The subduction was ultimately stopped by the ongoing continental collision between Eurasia and Arabia. The timing of the event has not been fully resolved, as some earlier studies have been inconclusive or even contradictory (Karimpour et al., 2011; Pang et al., 2013). However, a convergent setting is generally suggested to be associated with Late Cretaceous to Quaternary calc-alkaline and alkaline volcanism and syn- and post-tectonic granitoids (Camp & Griffis, 1982).

Paleogene (65–23 Ma) magmatic activity is evident in the area, which represents an Eocene-Oligocene (56-23 Ma) magmatic flare-up period (Pang et al., 2013). These rocks are dominated by intermediate compositions with calc-alkaline and high K-calc alkaline compositions. Pang et al. (2013) studied several samples collected from Eocene-Oligocene magmatic rocks in the Sistan suture zone to define their age, geochemical characteristic and petrogenesis. One sample (07-12) was obtained from the same circular structure studied in this work. Pang et al. (2013)'s sample was an andesite dated to 39.5+-0.6 Ma, containing plagioclase, hornblende, and biotite in a microgranular groundmass, similar to the samples investigated in this work.

2.2 Petrography

Four samples were collected from the Givshad circular structure, locally called Aghol Kuh. It is believed to be a collapsed caldera structure in the area (Khatib & Zarrinkoub, 2009), located at 32.653902°N and 59.077789°E (Figure 4).

Sample G1 (°N 32.656389, °E 59.084722): Porphyritic, phenocrysts and microphenocrysts of plagioclase and amphibole in microlite groundmass of plagioclase, quartz, and mafic minerals. The largest plagioclase phenocrysts are 2-2.5mm and exhibit complex zoning. Some microphenocrysts show no zoning or disequilibrium textures while others show patchy zoning with a different rim composition relative to the core. Different optic characteristics for tabular plagioclase cores were also observed. Amphiboles range from 0.5-2.5mm.

Sample G2 (°N 32.652222, °E59.083056): Porphyritic, largest plagioclase phenocrysts up to 1.5-2 mm have complex zoning (as in sample G1). The crystal habit of all crystal populations is commonly tabular, although some microphenocrysts (0.5-1 mm) are euhedral, crystals smaller than 0.5 mm are generally equant. Dif-

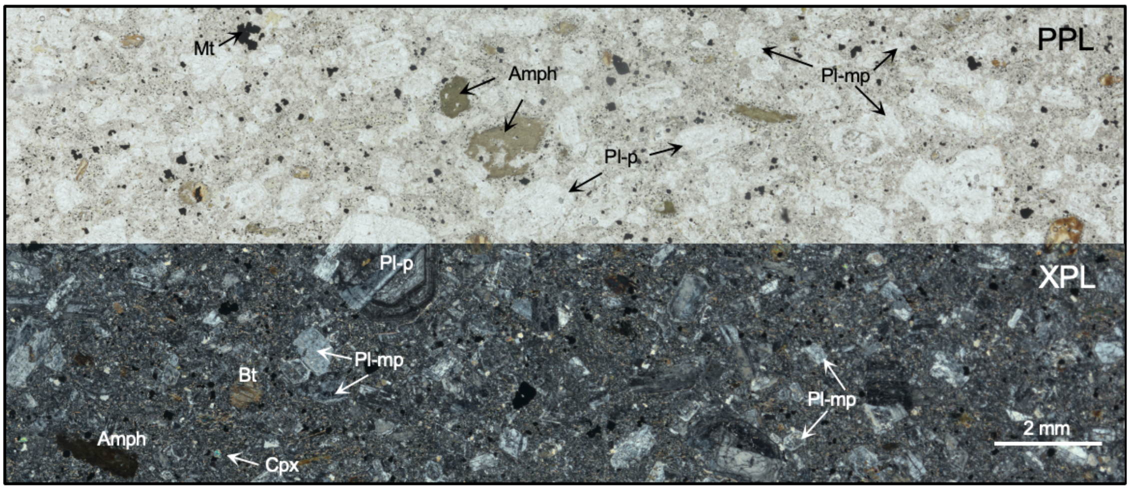

Figure 3: Mineralogy of sample G2, Pl divided into microphenocrysts (mp) and phenocrysts (p). Pl = plagioclase, Amph = amphibole, Bt = biotite, Cpx = clinopyroxene.

ferent types of zoning are visible in all sizes. Amphibole is present in the matrix and as phenocrysts 0.5-2.5mm in size. Other minerals observed include pyroxene (as microphenocrysts), and biotite- and chlorite-alterations.

Sample G3 (°N 32.650278, °E 59.079444): Porphyritic, with the largest phenocrysts (plagioclase and amphibole) 2-2.5mm in size. Phenocryst populations of 1-1.5mm show polysynthetic twinning + oscillatory zoning. Some crystals exhibit both textures while others have only one. Resorption textures are seen in some plagioclase crystals having rounded uniform cores with sharper oscillatory zoned layers in an euhedral rim. Microphenocrysts are generally euhedral or tabular.

Sample G4 (°N 32.649722, °E 59.072778): Porphyritic, with the largest plagioclase phenocrysts 2-2.5mm. These often show oscillatory or complex zoning, while others only show polysynthetic twinning. Glomerocrysts occur in all size populations. Phenocrysts may have spongy/sieve textures. Groundmass consists of plagioclase, k-feldspar, quartz and mafic minerals. Most of the plagioclase crystals are euhedral and yellow-hued, the latter indicative of alteration.

All samples are fine-grained and porphyritic. They have a composition ranging from 50-60% plagioclase, 10-15% amphibole and accessory (<5%) minerals such as biotite, pyroxene, apatite, magnetite, k-feldspar and quartz (Figure 3). Some alterations occurs in plagioclase, amphibole, and biotite. The mineralogy of the groundmass includes both feldspars, mafic minerals, and interstitial quartz. Plagioclase and amphibole appear to be the primary mineralogy, occurring in both the matrix and as phenocrysts up to 2.5mm. Crystal abundance is much higher for plagioclase relative to the amphiboles. Moreover, crystal habits for the large plagioclase show both equilibrium and disequilibrium textures such as oscillatory zoning, complex zoning, and spongy textures (Figure 2). Patchy zoning, aggregates, and equant habits are relatively more common in the smaller microphenocrysts but occur in both populations. Generally, optical properties of microphenocrysts (0.2-1mm) consistently observed were the tabular or equant crystal habits, a few were rounded indicating resorption. The phenocrysts (1-2.5mm) are generally euhedral to subhedral.

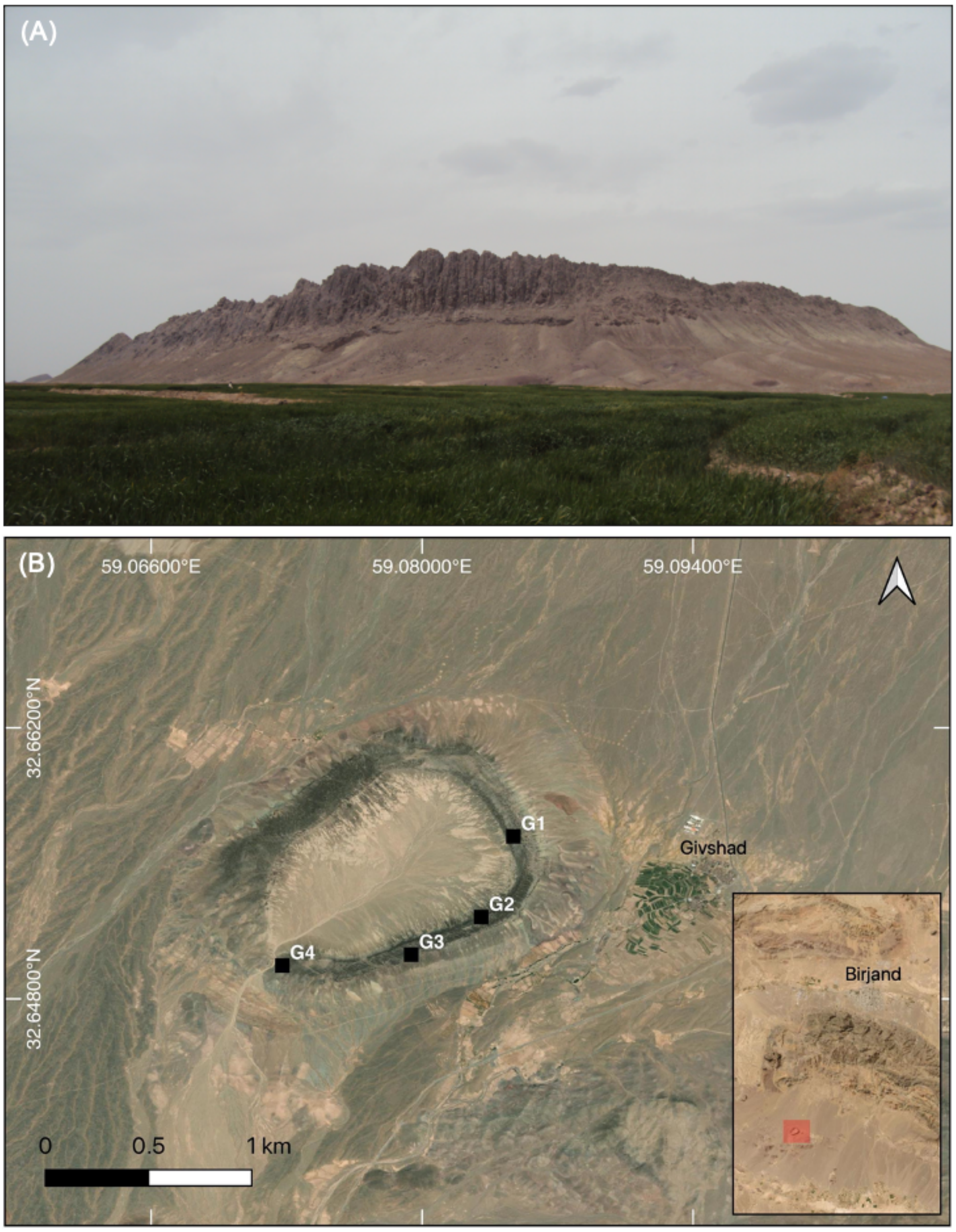

Figure 4: Givshad circular structure (Aghol Kuh). (A) Photo by Fazilat Yousefi. (B) Map of study area with sample locations. Source: ESRI

Methods

Rock samples were collected from Aghol Kuh near Givshad village in Eastern Iran (provided by E. Yousefi). These were prepared for both microscopy studies and chemical analysis prior to this study. The methods applied here utilize petrographic analysis with a Leica microscope, shareware ImageJ to integrate textural analysis and CSDCorrections and ShapeCalc software for CSD analysis, and chemical data acquired by a scanning electron microscope (SEM) equipped with energy-dispersive X-ray spectroscopy (EDS).

3.1 Crystal Size Distribution

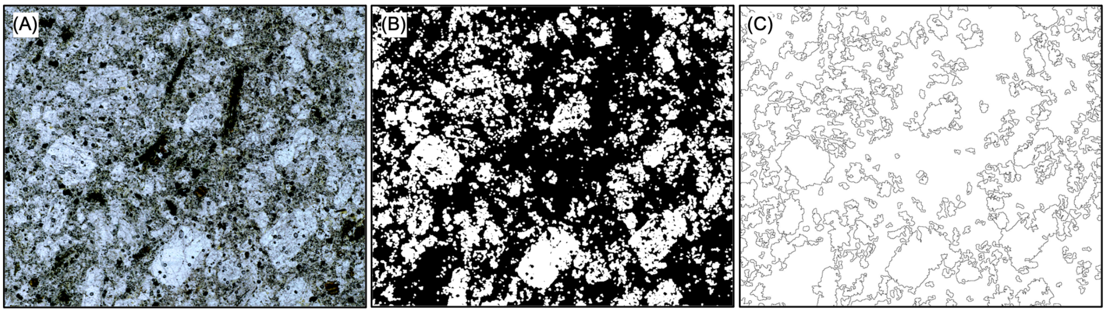

Figure 5: Image processing in ImageJ. (A) Digitized sample (PPL). (B) Thresholded image highlighting plagioclase. (C) Outlines of plagioclase crystals.

Crystal size distributions of plagioclase in four thin sections were measured using optical and analytical methods following Higgins guide for CSD analysis (Higgins, n.d., 2000). The thin sections were scanned with a Nikon Coolpix 9000 Scanner, and images were digitally stitched together using Panorama Stitcher since the thin sections were too long to fit the scanning slides for a single session. The digitized samples were processed in ImageJ to produce a binary (black and white) image, allowing the software to automatically trace crystal outlines to calculate the position, orientation, and dimensions of a best-fit ellipse for each outline (Figure 5).

The scale was determined for each sample before calculating 2D measurements. The results were saved as a .csd file, to finally run in CSDCorrections which requires image area, crystal habit, and foliation inputs. 3D crystal shape estimates were obtained by ShapeCalc after Mangler et al. (2022). Since multiple crystal habits cannot be set by the program, aspect ratios were estimated to 1:1:1.55 without any roundness. A massive fabric was used since no apparent orientation of the plagioclase crystals could be observed. Weak fabrics will have minor effects on CSD calculations according to Higgins and Chandrasekharam (2007). The authors also suggested removing size bins with fewer than two crystals to avoid inaccuracies. Observed aggregates included in the large-size bins were also cleared, to further minimize potential misconceptions. Crystals larger than 0.04 mm^2 have been accounted for, smaller ones have been observed but not measured. The CSDs for crystals smaller than this size are therefore undefined. This limit is due to technical considerations where some crystals are too small to be accurately recognizable by ImageJ.

3.2 Geochemical Analysis

Geochemical composition was acquired by a FEI Quanta 650 field-emission scanning electron microscope (SEM), fitted with a 80mm^2 X-MaxN Oxford Instruments EDS detector (20kV, beam size >1µm, working distance 10mm) installed at Swedish Natural Museum. The instrument was calibrated using cobolt and point analyses was set to 10. The instrument uses an electron backscatter diffraction (EBSD) technique which enables a full characterization of a sample's microstructural properties. The samples occupied an area of 11x13mm and were carbon-coated prior to the analysis, to increase reflectivity and prevent charging mechanisms.

Energy-dispersive X-ray spectroscopy (EDS) is a semi-quantitative technique that provides relative elemental compositions by detecting characteristic X-rays emitted by a sample once it is charged with an electron beam. Data acquisition of plagioclase crystals between 0.2-2mm were analyzed in Aztec (Figure 6). Recalibration of the instrument was required several times due to beam strength irregularities. Total compositions rarely reached 100±1 wt% but were normalized to present cohesive results. For each sample, 15-30 images were collected to construct montaged elemental maps (Figure 6C).

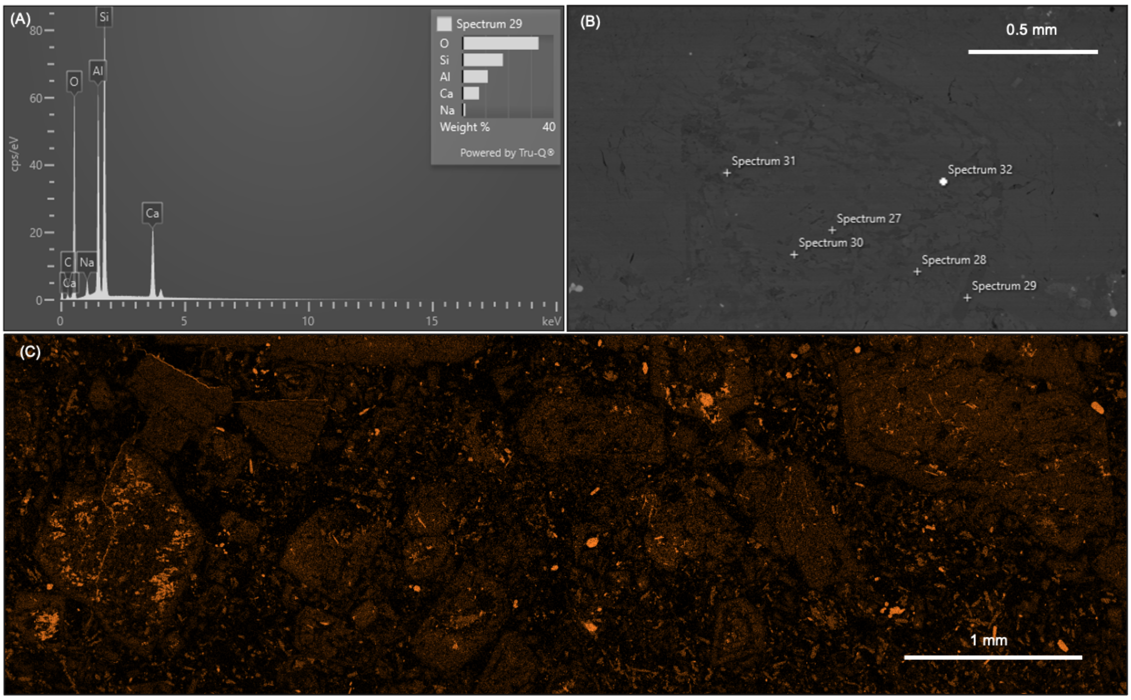

Figure 6: SEM-EDS analysis in AZtec. (A) Elemental compositions for spectrum 29. (B) EBSD image of spectrum points in sample (G4_3), dark hues indicating relatively light elements. (C) X-ray map of Ca, brightness indicating richer calcic compositions.

Results

4.1 CSD Analysis

The CSD analysis reveal non-linear (kinked) trends for all samples. Two distinct populations are characterized by linear regression segments in each plot (Figure 7), coincident with microphenocrysts (long axis $< \sim 1$ mm) and phenocrysts (long axis $> \sim 1$ mm). The grey area between the two trends defines the break between population sizes, the actual size division lies within this area. The largest frequency prevalent is the smaller microphenocryst population (Table 1). Comparatively, the large population shows decreasing frequency relative to increasing crystal size. Slopes are steeper for the microphenocrysts in comparison to the phenocryst. This indicates two different nucleation events.

Table 1: Crystal size distribution results from CSDCorrections

G1			G2			G3			G4		
Size interval	Frequency	Area (mm^2)	Size interval	Frequency	Area (mm^2)	Size interval	Frequency	Area (mm^2)	Size interval	Frequency	Area (mm^2)
2.51	19	1161	2.51	25	1411	2.51	17	891	2.51	15	1045
1.58	68		1.58	70		1.58	60		1.58	59	
1.00	141		1.00	190		1.00	118		1.00	106	
0.63	268		0.63	427		0.63	309		0.63	189	
0.40	450		0.40	700		0.40	585		0.40	450	
0.25	842		0.25	1085		0.25	1096		0.25	767	

4.2 SEM-EDS Analysis

Summary of results are compiled and presented in Table 2, where rows represent individual crystals within all four samples. The cores of the phenocryst population range from 8-13 % CaO which is on average, higher Ca than in the microphenocrysts (2-15 % CaO) (Figure 8). Strong correlation between cores and rims relative to crystal length are not apparent, since crystals within each population exhibit multiple tendencies. In sample G1-G2, microphenocrysts show decreasing Ca- trends from core to rim (Table 2). The exception are crystals with patchy zoning or chemical disequilibrium, that illustrate the opposite trend. However, in sample G3 the majority of the microphenocrysts show enriching Ca-trends from core to rim, with changes ranging from an increase of 5% - 308%. Almost a third of these crystals exhibit spongy textures or patchy cores, while the rest do not display disequilibrium textures. Nearly half of the analyzed crystals in G4 show enriching CaO-trends from core to rim in both populations. The X-ray maps reveal complex compositional trends in both populations (Figure 9), similar to the EDS spectrum data. The larger crystals have either uniform composition, oscillatory zoning or complex zoning. Sieve textures are common in the 0.8-1mm size range.

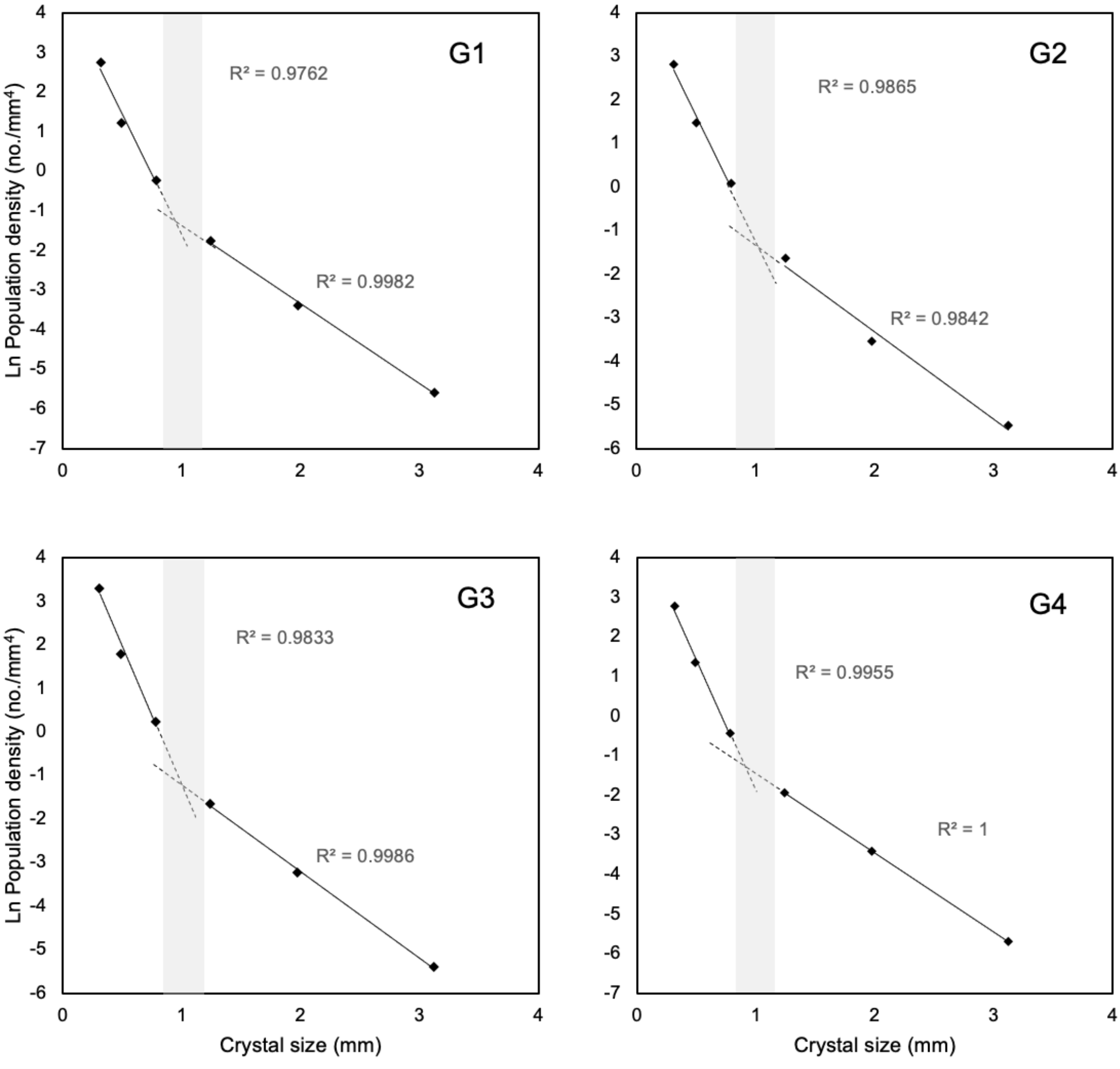

Figure 7: CSDs for plagioclase phenocrysts in all four samples. Grey band represents break between microphenocrysts and phenocrysts.

Table 2: EDS-results

Sample	Crystal/Spectrum	Core (CaO%)	Mid (CaO%)	Rim (CaO%)	Change C-M (%)	Change C-R (%)	C. length (mm)
	mp1920	9.92		3.30		-67	0.40
	mp2123	8.00		6.04		-24	0.35
	mp3233	11.25		7.43		-34	0.30
	mp4847	10.49		9.88		-6	0.50
	mp5049	9.21		4.77		-48	0.70
	mp5253	8.27		4.31		-48	0.60
G1	mp6667	7.63		5.27		-31	0.70
	mp7475	12.15		5.04		-59	0.20
	mp7677	1.80		9.61		434	0.20
	mp292830	10.71	11.98	7.51	12	-30	0.23
	mp62	8.55					0.20
	p2726	10.08		11.95		19	1
	p61		9.69				1
	p63		8.17				1
	mp1314	9.80		8.76		-11	0.30
	mp46*	8.63		11.21		30	0.20
	mp3536	9.30		7.16		-23	0.40
	mp4544	13.50		9.75		-28	0.30
	mp5957	10.94		6.28		-43	0.27
G2	mp6263	8.66		2.33		-73	0.25
	mp88	2.28					0.20
	mp90	5.17					0.40
	mp252726	9.61	6.75	10.37	-35	8	0.60
	p1112	8.91		3.04		-66	1
	p7980	11.98		7.71		-36	1
	mp111214*	9.42	10.69*	9.69	13	3	0.58
	mp151617†	2.82	25.00*	9.19	788	226	0.44
	mp181920†	2.74	6.86	11.19	150	308	0.56
	mp686766†	2.89	10.07	10.28	248	255	0.40
G3	mp3132	6.90		8.13		18	0.40
	mp3738	2.93		9.35		219	0.50
	mp4748	8.61		9.39		9	0.48
	mp4950	11.32		9.03		-20	0.55
	mp5657	10.66		9.55		-10	0.45
	mp878889†	9.18	5.31*	10.09		10	0.87
	p424345	12.72	11.13	9.97		-22	1
	mp68	12.13		10.09		-17	0.20
	mp4039†	2.64		11.75		346	0.25
	mp6970	9.22		6.34		-31	0.40
	mp141617	9.59	10.84	1.30	13	-86	0.30
	mp596061	10.67	11.04	10.97	3	3	0.70
	mp626364	8.26	9.03	6.78	9	-18	0.37
G4	mp717275	9.66	1.46	9.05	-84	-6	0.80
	mp818283	14.80	10.63	7.27	46	-51	0.37
	p272829‡	10.24	11.94	14.36	17	40	1.4
	p333437†	10.11	3.15	11.54	-69	14	2.25
	p414344	8.93	9.33	8.77	5	-2	1
	p505153	9.53	8.39	10.27	-12	8	1.4
	p848586	13.26	9.49	9.23	-28	-30	1

mp = microphenocryst, p = phenocryst
*disequilibrium relations
†spongy or patchy textures
‡skeletal textures

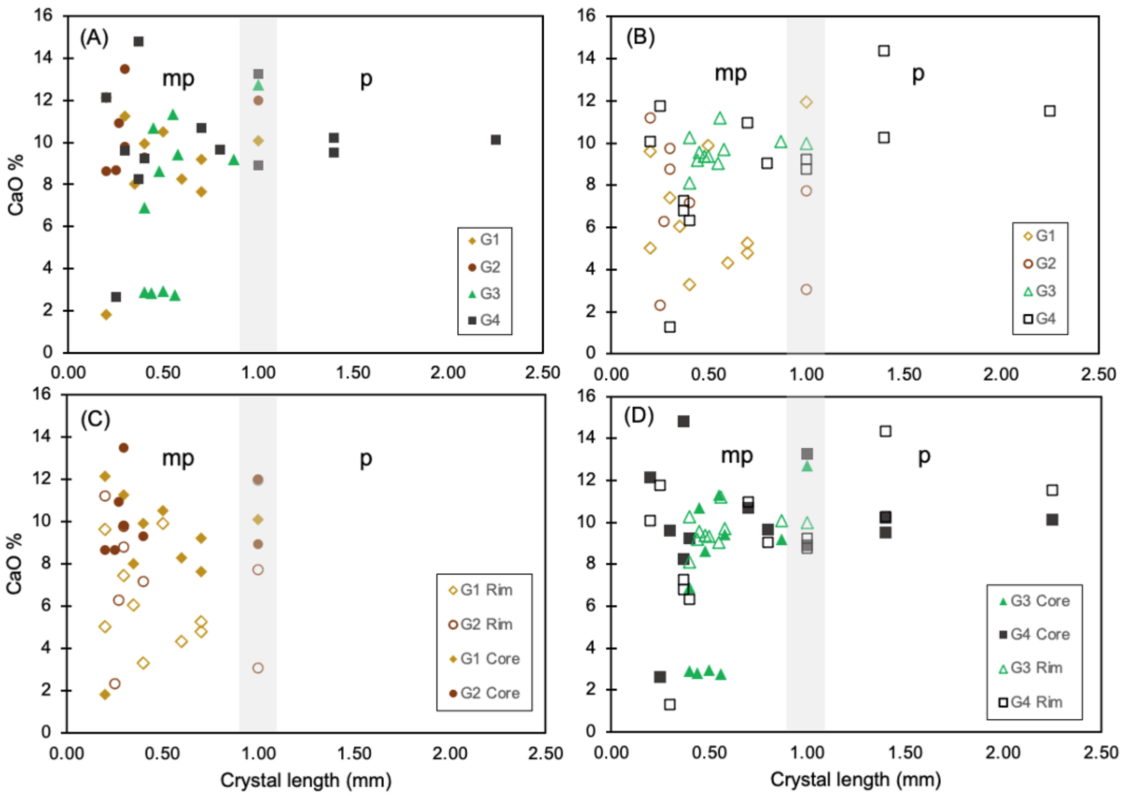

Figure 8: EDS-results of CaO % in different size crystals measured in ImageJ. The vertical grey area represents the interval of division between two populations, microphenocrysts (mp) to the right and phenocrysts (p) to the left. (A) CaO % in cores plotted against crystal length. (B) CaO % in rims plotted against crystal length. (C) Cores and rims of crystals in G1 and G2. (D) Cores and rims of crystals in G3 and G4.

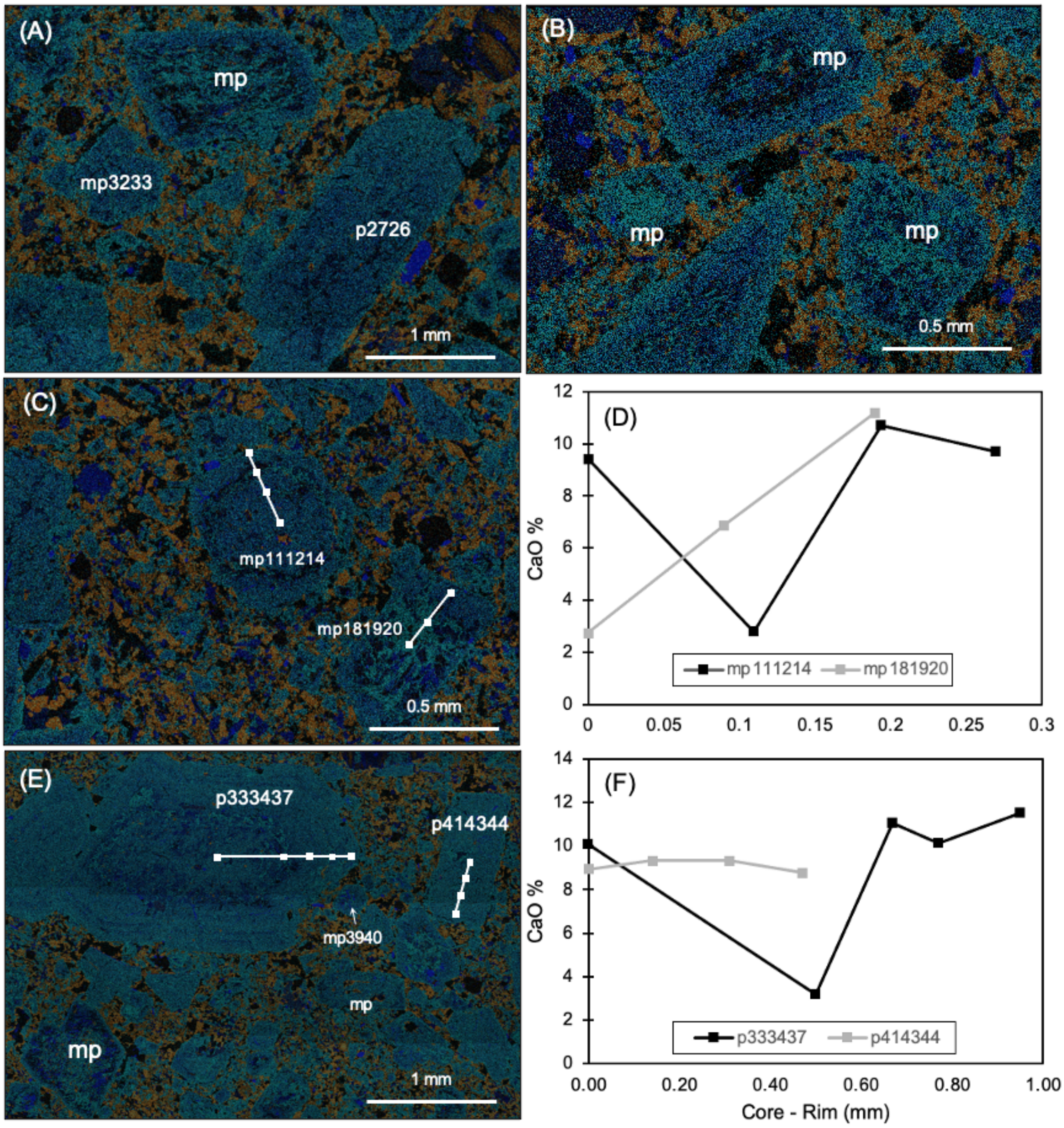

Figure 9: Elemental maps illustrating Ca (navy), Na (blue), and K (orange). (A) G1, microphenocryst (mp) with spongy texture. (B) G1, representative tabular mp with spongy and patchy core along with other crystals. (C) G3, mantle disequilibrium in crystal mp111214. Calcic mantle on sodic core in mp181920. CaO composition illustrated in (D) reveals multiple trends within a single sample. Crystal mp111214 shows a complex compositional variation, while crystal mp181920 shows increasing CaO from core to rim. (E) G4, phenocrysts (p) populations with distinct composition. Mps show sieve texture, patchy zoning and reverse zoning. The largest phenocryst crystal (p333437) has spongy textures with a complex chemical evolution while another crystal (p414344) shows a uniform composition (F).

Discussion

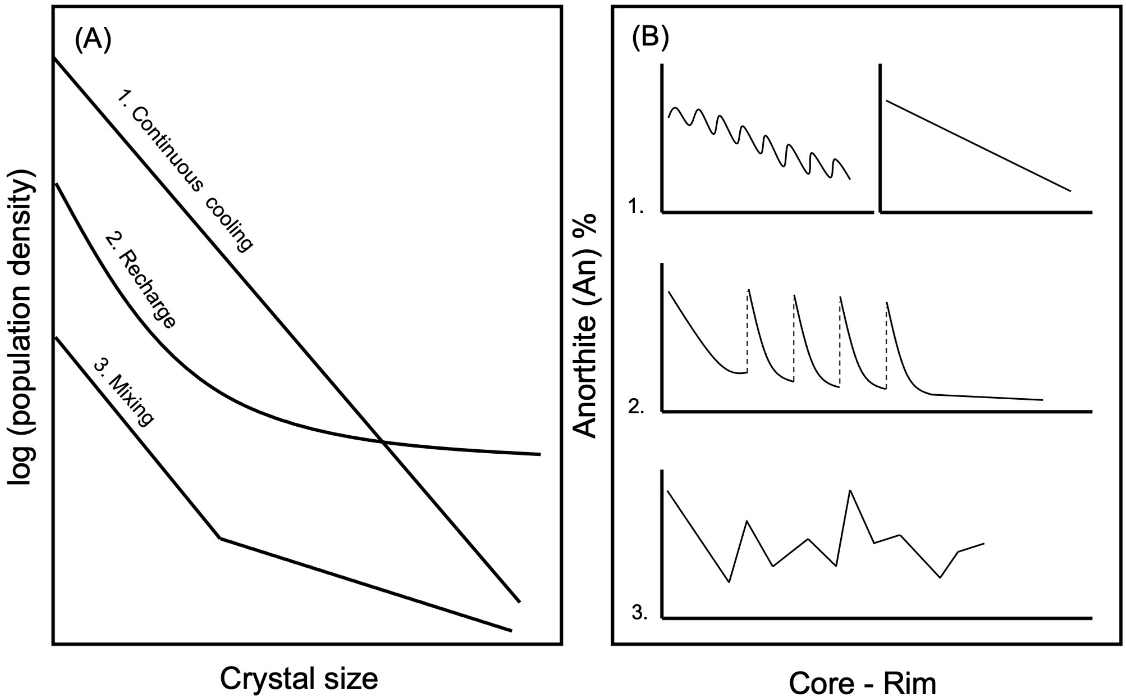

Figure 10: Possible CSD trends and plagioclase geochemical correlation. (A1.) Continuous cooling in equilibrium systems correlates with (B1.), steady-state compositional variation. (A2.) Mafic recharge in open systems yield (B2.) periodic disequilibrium conditions (Higgins & Roberge, 2003). (A3.) Magma mixing defines different nucleation events related to (B3.), where intricate chemical patterns align with complex zoning, patchy zoning, or spongy textures (Salisbury et al., 2008).

5.1 Integration of CSD and EDS

Since CSD trends can be established and interpreted in different ways (Figure 10), geochemical analysis is important for determining accurate assessments. In this case, the results given by CSDCorrections could be interpreted as a polynomial trend, an indication of magma recharge not necessarily involving magma mixing (Higgins & Roberge, 2003). However, since the geochemical data for the plagioclases exhibit at least two different compositional trends suggesting both equilibrium and non-equilibrium conditions, this is unlikely and supports the interpretation of not one, but multiple different nucleation events (n^0), to generate the non-linear (kinked) trends documented here.

All four samples contain two crystal size populations and there is a clear distinction of higher average CaO contents in the phenocrysts relative to the microphenocrysts. The distinction between the two size populations involves a wider CaO-range for the microphenocrysts' cores relative to the phenocrysts', with CaO contents ranging from 1.8-14.4% and 8.9-13% respectively. It appears that there is a tendency for higher calcic values in cores for the large population, which do not display values smaller than 8 %. Except for this, there is no apparent trend correlating Ca-content and crystal length. All crystal populations (microphenocrysts and phenocrysts) show small compositional fluctuations typical of oscillatory zoning (Figure 9). Moreover, in sample G3 some crystals ranging from 0.4-0.6 mm reveal relatively increasing Ca from core to rim (Figure 9D). The EDS results and X-ray maps indicate diverse plagioclase populations with variable compositions within each of the two crystal size populations identified by CSD analysis. Additionally, given that the microlite populations were too small to be included in this study, it is possible that an additional crystal population(s) is present in these samples.

5.2 Magmatism of the Givshad structure

As mentioned earlier, the cyclic structure is suggested to be associated with a collapsed caldera, and its magmatism is believed to be related to several different tectonic interpretations (Khatib & Zarrinkoub, 2009; Pang et al., 2013). Multiple plagioclase crystal populations indicate one or two magma mixing events, indicated by diverse internal compositional variations. This aligns with observed plagioclase disequilibrium textures in thin sections (such as skeletal growth and patchy zoning) and non-equilibrium compositional variations identified by EDS analysis. These observations are likely attributed to a mafic recharge event, involving the injection of a hotter (more CaO-rich) magma into an existing, cooler magma body, which potentially could trigger an eruption event (Morgavi et al., 2017). This would account for the variable plagioclase compositions, reversed and irregular compositional zoning, and is reinforced by the micro granular groundmass, which opposes rapid magmatic cooling or a fast ascent rate.

5.3 Future work

Challenges related to this study are mostly associated with the SEM-EDS analysis. Since the largest phenocrysts (2-2.5mm) are relatively rare in these samples, a more practical approach would involve initial optical microscopy of the thin sections to decide on a specific area to be analyzed before the preparation of SEM-EDS specimens. By using this approach, the study could have optimized the use of resources and ensured a more efficient analysis of the desired populations of interest. Since the SEM-EDS samples were prepared prior to this study, some of them did not contain representative grains of the size populations observed in the thin sections.

Additionally, when acquiring spectrum data, distinguishing crystals and their outlines from the groundmass is not straightforward. EBSD-imaging shows no apparent contrast between plagioclase phenocrysts and the groundmass, which complicates selecting proper locations for analysis. Improvements could include other imaging techniques, such as Nomarski imaging, combined with a fluorobaric acid treatment which dissolves Ca-rich zones in plagioclase to produce microtopographic relief to reveal sodic highs and calcic lows (Salisbury et al., 2008). This would improve the efficiency of data acquisition, since textures and outlines become more apparent. Using quantitative analysis, such as an electron microprobe (EMP), would yield a better determination of mineral compositions from core-rim and provide a more useful understanding of the geochemical evolution of plagioclase crystallization trends. In addition, including microlites in the analysis might improve the final interpretation of the results as it would yield a more comprehensive assessment. Other studies often incorporate isotopic and trace elemental analysis to further reinforce a conclusion (Perugini & Poli, 2012; Salisbury et al., 2008). Moreover, to determine a solid conclusion, further analyses are needed to conduct a statistically significant correlation between the plagioclase size distribution and their chemical diversity.

Other challenges are related to the CSD-measurements. For aggregates or crystals adjacent to each other, ImageJ would measure them as one single crystal. Apparent aggregates were removed for this reason, and not included in the CSD analysis. Since the measured crystal frequency was roughly 1500-2000, it should not have significantly affected the result. However, it is still advised to trace crystal outlines manually and then integrate ImageJ for automated measurements to ensure the quality of the CSD data.

5.4 Conclusions

Petrographic studies combined with geochemical data and crystal size distribution analysis of plagioclase populations in four samples from Aghol Kuh near Givshad revealed the presence of at least two distinct plagioclase populations in these volcanic rocks. This combined data provide evidence of magma mixing prior to the volcanic eruption. Furthermore, the occurrence of a mixing event could have triggered the final eruption. To strengthen this conclusion, additional quantitative geochemical investigations are recommended, particularly incorporating isotopic and trace elemental analysis. Such studies would provide valuable insights into identifying magma mixing processes, which can be further utilized when optimizing mitigation against volcanic eruptions.

Acknowledgements

I would like to thank my supervisor Victoria Pease who has guided me with patience and positivity during this time, your careful advice and review genuinely improved the quality of this work. Special thanks to Esmail Yousefi for kindly lending me the samples, and Fazilat Yousefi for providing photographs of the volcanic structure at short notice. I am also grateful to the institution for their financial support and to the professors that have kept me inspired during the course of my education.

I would also like to express special gratitude to friends and family for supporting me, and for allowing me time to focus on finalizing my degree.

Finally, earnest thanks to my partner Stef. I probably would not have reached this point without you. I will always be grateful for your love, patience and invaluable support.

References

Boorman, S., Boudreau, A., & Kruger, F. (2004). The lower zone-critical zone transition of the bushveld complex: A quantitative textural study. *Journal of Petrology - J PETROL*, *45*, 1209–1235. https://doi.org/10.1093/petrology/egh011

Bröcker, M., Hövelkröger, Y., Berndt, J., Scherer, E., Kurzawa, T., & Moslempour, M. E. (2022). The magmatic and tectono-metamorphic history of the sistan suture zone, iran: New insights into a key region for the convergence between the lut and afghan blocks. *Journal of Asian Earth Sciences*, *236*, 105313. https://doi.org/10.1016/j.jseaes.2022.105313

Camp, V., & Griffis, R. (1982). Character, genesis and tectonic setting of igneous rocks in the sistansuture zone, eastern iran. *Lithos*, *15*(3), 221–239. https://doi.org/10.1016/0024-4937(82)90014-7

Cashman, K. (2020). Crystal size distribution (csd) analysis of volcanic samples: Advances and challenges. *Frontiers in Earth Science*, *8*. https://doi.org/10.3389/feart.2020.00291

Cashman, K., & Marsh, B. (1988). Crystal size distribution (csd) in rocks and the kinetics and dynamics of crystallization ii: Makaopuhi lava lake. *Contributions to Mineralogy and Petrology*, *99*, 292–305. https://doi.org/10.1007/BF00375363

Hibbard, M. (1981). The magma mixing origin of mantled feldspar. *Contributions to Mineralogy and Petrology*, *76*, 158–170. https://doi.org/10.1007/BF00371956

Higgins, M., & Roberge, J. (2003). Crystal size distribution of plagioclase and amphibole from soufriere hills volcano, montserrat: Evidence for dynamic crystallization-textural coarsening cycles. *Journal of Petrology - J PETROL*, *44*, 1401–1411. https://doi.org/10.1093/petrology/44.8.1401

Higgins, M. (n.d.). *A quick guide to thin section / slab digitization*. http://www.uqac.ca/mhiggins/Quick_thin_section_digitisation.htm (accessed: 24.04.2023)

Higgins, M. (2000). Measurement of crystal size distributions. *American Mineralogist*, *85*, 1105–1116. https://doi.org/10.2138/am-2000-8-901

Higgins, M. (2006a). *Quantitative textural measurements in igneous and metamorphic petrology*. Cambridge University Press. https://doi.org/10.1017/CBO9780511535574

Higgins, M. (2006b). Verification of ideal semi-logarithmic, lognormal or fractal crystal size distributions from 2d datasets. *Journal of Volcanology and Geothermal Research - J VOLCANOL GEOTHERM RES*, *154*, 8–16. https://doi.org/10.1016/j.jvolgeores.2005.09.015

Higgins, M., & Chandrasekharam, D. (2007). Nature of sub-volcanic magma chambers, deccan province, india: Evidence from quantitative textural analysis of

plagioclase megacrysts in the giant plagioclase basalts. *Journal of Petrology*, *48*. https://doi.org/10.1093/petrology/egm005
Jaret, S., Mayne, R., & McSween, H. (2008). Demystifying crystal size distribution (csd): A comparison of methodologies using eucrite meteorites. *Lunar and Planetary Science Conference*, 1487.
Karimpour, M. H., Stern, C., Farmer, L., Saadat, S., & Malekzadeh Shafaroudi, A. (2011). Review of age, rb-sr geochemistry and petrogenesis of jurassic to quaternary igneous rocks in lut block, eastern iran.
Khatib, M., & Zarrinkoub, M. (2009). Morpho-tectonics and mechanism of emplacement of the andesitic ring in givshad, east of iran [Accessed: 28-5-2023].
Marsh, B. (1988). Crystal size distribution (csd) in rocks and the kinetics and dynamics of crystallization. *Contributions to Mineralogy and Petrology*, *99*(99), 277–291. https://doi.org/10.1007/BF00375362
Marsh, B. (1998). On the interpretation of crystal size distributions in magmatic systems. *Journal of Petrology*, *39*. https://doi.org/10.1093/petroj/39.4.553
Morgan, D. J., & Jerram, D. A. (2006). On estimating crystal shape for crystal size distribution analysis. *Journal of Volcanology and Geothermal Research*, *154*(1-2), 1–7. https://doi.org/10.1016/j.jvolgeores.2005.09.016
Morgavi, D., Arienzo, I., Montagna, C., Perugini, D., & Dingwell, D. B. (2017). Magma mixing: History and dynamics of an eruption trigger. In J. Gottsmann, J. Neuberg, & B. Scheu (Eds.), *Volcanic unrest*. Springer. https://doi.org/10.1007/11157_2017_30
Nelson, S., & Montana, A. (1992). Sieve-textured plagioclase in volcanic rocks produced by rapid decompression. *American Mineralogist*, *77*, 1242–1249.
Pang, K.-N., Chung, S.-L., Zarrinkoub, M., Khatib, M., Mohammadi, S. S., Chiu, H.-Y., Chu, C.-H., Lee, H.-Y., & Lo, C.-H. (2013). Eocene-oligocene post-collisional magmatism in the lut-sistan region, eastern iran: Magma genesis and tectonic implications. *Lithos*, *180*, 234–251. https://doi.org/10.1016/j.lithos.2013.05.009
Perugini, D., & Poli, G. (2012). The mixing of magmas in plutonic and volcanic environments: Analogies and differences. *Lithos*, *153*, 261–277. https://doi.org/10.1016/j.lithos.2012.02.002
Salisbury, M., Bohrson, W., Clynne, M., Ramos, F., & Hoskin, P. (2008). Multiple plagioclase crystal populations identified by crystal size distribution and in situ chemical data: Implications for timescales of magma chamber processes associated with the 1915 eruption of lassen peak, ca. *Journal of Petrology*, *49*. https://doi.org/10.1093/petrology/egn045
Vance, J. (1965). Zoning in igneous plagioclase: Patchy zoning. *Journal of Geology - J GEOL*, *73*, 636–651. https://doi.org/10.1086/627099
Vernon, R. (2004). *A practical guide to rock microstructure*. Cambridge University Press.
Wager, L. (1961). A note on the origin of ophitic texture in the chilled olivine gabbro of the skaergaard intrusion. *Geological Magazine*, *98*, 353–364. https://doi.org/10.1017/S0016756800060829

Appendix

Appendix including X-ray elemental maps, raw data of spectrum analysis (EDS), and CSD analysis have been excluded for brevity. Additional material is available upon request to the author.